


**Wave propagation in head
impact response**
Assessment of physical possibility
and numerical artifacts.

D.W.A. Brands.
WFW reportnr. 99.005

 Eindhoven University of Technology,
Faculty of Mechanical Engineering,
Dept. of Computational and Experimental Mechanics,
February, 1999.



Summary

Theory on three dimensional wave propagation through semi-infinite elastic media has been presented. Simulation of wave phenomena with the Finite Element Method introduces numerical artifacts, dispersion and spurious reflection. It can be derived analytically that these errors depend on the relative mesh size, i.e. the number of elements per wavelength. Two dimensional dispersion analysis, valid for both dilatational (Pressure) and distortional (Shear) single frequency waves, shows that the use of 18 constant strain elements per wavelength leads to a 1% underestimation of the wave propagation velocity. Applying this relative mesh size in non-uniform meshes gives a reflected wave with an amplitude of 2.5 % of the incident wave. In current FE-head models the element size is typically 0.01 m . This means that the wave length that can be described accurately is about 0.18 m which corresponds to the typical size of a 50th percentile head. It is very unlikely that that wave propagation can be described accurately in current headmodels.

For gaining insight if this is realistic the propagation of a one-dimensional P-wave in a linear elastic beam has been modelled in MADYMO using a realistic, traffic impact like, input pulse. P-wave has been investigated as to obtain a true one dimensional problem which analytically shows no dispersion. A difficulty in the analysis was that single frequency waves do not exist in reality. The analysis showed that in this one-dimensional problem approximately 16 elements per maximum wavelength were needed to obtain a dispersion error of less than 1%. The strain error with respect to the maximum strain after having traveled 30 m than equals 10%. If the code behaves the same for S-waves, as expected theoretically, an element size of $2.5 \cdot 10^{-3} m$ is needed for a dispersion error less than 1%. The strain error than will be 10% at 0.1 m wave traveling distance. This means that the number of elements needed in a head model will be $4^3 = 64$ times the number of elements used in current state of the art models. For the three dimensional case it can be estimated that this will be 175 times as much.

The presence of certain wave types in the head is also investigated. A lower bound can be defined by considering the wavelength for which a wavelength fits inside a typical head measure (i.e. $\lambda_{max} \leq D_{head} = 0.2 m$). This means that P-waves exist for $f > 7750 Hz$, while S-waves exist at $f < 25 Hz$. The upperbound of the relevant frequency range is determined by the viscoelastic properties of brain tissue. For S-waves the upperbound is estimated to be 300 Hz . For P-waves the damping is that small that the upperbound will be determined by the excitation frequency.

It is shown that an upperbound for the frequency in typical traffic related impacts equals 3750 Hz . For this reason no P-waves will be present but S-waves will. In a ballistic/forensic blunt impact situation first a direct impact with a duration of approximately 2 to 100 μs [22],[23] will occur. After this inertia will cause the head to rotate with a typical duration of order ms [24]. This means that P-waves can be present at the start and S-waves might develop later on.

Contents

1	Elementary theory on elastic wave propagation	7
2	Numerical simulation of elastic wave propagation: theoretical considerations	11
2.1	Numerical stability	11
2.2	Numerical accuracy	11
2.3	Implications for existing head models	14
2.4	Methods of improvement	14
2.5	Conclusions	15
3	Numerical simulation of elastic wave propagation: MADYMO computation	17
3.1	Analytical solution of the 1D wave equation	17
3.2	The numerical model	17
3.2.1	Discretisation requirements	18
3.3	Results	19
3.4	Parametric study	19
3.5	Conclusions and discussion	22
4	Importance of wave phenomena in the human head	25
4.1	Boundary conditions for wave propagation	25
4.2	Effect of damping	25
4.3	2D Reflection	27
4.4	Summary and Conclusions	29
5	Discussion and conclusions	31
5.1	Presence of wave propagation during head impact	31
5.2	Implications for accuracy of existing head models.	31
	Bibliography	33

Chapter 1

Elementary theory on elastic wave propagation

Elementary theory on wave propagation in semi-infinite, isotropic, linear elastic media will be presented as done in e.g.[1].

In absence of body forces the general three dimensional equations of motion are given by,

$$\nabla \cdot \boldsymbol{\sigma} = \rho \frac{\partial^2 \vec{u}}{\partial t^2} \quad (1.1)$$

where ρ is the mass density of the material, $\boldsymbol{\sigma}$ the symmetric Cauchy stress tensor, t the time, and \vec{u} the displacement vector. Small deformations theory will be applied. For this reason the Green-Lagrange strain will be linearised into linear strain, according to,

$$\boldsymbol{\epsilon} = \frac{1}{2} ((\nabla \vec{u})^c + (\nabla \vec{u})) \quad (1.2)$$

Linear elastic material behaviour now can be described using Hooke's law given by,

$$\boldsymbol{\sigma} = \lambda \text{trace}(\boldsymbol{\epsilon}) \mathbf{I} + 2\mu \boldsymbol{\epsilon} \quad (1.3)$$

where λ and μ are the Lamé parameters for the material. Substitution of Hooke's law into Equation(1.1) gives us the Navier equations for the medium,

$$(\lambda + \mu) \nabla (\nabla \cdot \vec{u}) + \mu \nabla^2 \vec{u} = \rho \frac{\partial^2 \vec{u}}{\partial t^2} \quad (1.4)$$

By applying the vector identity,

$$\nabla^2 \vec{u} = \nabla (\nabla \cdot \vec{u}) - \nabla \times (\nabla \times \vec{u})$$

and introducing both dilatation Δ , which represents the change in volume of the material,

$$\Delta = \nabla \cdot \vec{u}$$

and rotation $\vec{\omega}$ [14],

$$\vec{\omega} = \frac{1}{2} (\nabla \times \vec{u})$$

equation(1.4) can be rewritten as,

$$(\lambda + 2\mu) \nabla \Delta - 2\mu \nabla \times \vec{\omega} = \rho \frac{\partial^2 \vec{u}}{\partial t^2} \quad (1.5)$$

which is the three dimensional wave equation for unbounded linear elastic media. It can be shown that this set of equations describes the propagation of two types of waves through the

medium: waves of distortion or S-waves, in which particle motion occurs perpendicular to the direction of propagation of the wave, and waves of dilatation or P-waves, which correspond with the change of volume.

The dilatational wave equation can be derived by taking the divergence of equation(1.5),

$$\nabla^2 \Delta = \frac{1}{c_p^2} \frac{\partial \Delta}{\partial t^2} \quad (1.6)$$

with $\nabla^2 \equiv \nabla \cdot \nabla$ and c_p the propagation velocity of the P-wave which equals,

$$c_p = \sqrt{\frac{\lambda + 2\mu}{\rho}} \quad (1.7)$$

The wave-equation for the distortional waves can be derived by taking the cross-product of the gradient operator and equation(1.5). This yields,

$$\nabla^2 \vec{\omega} = \frac{1}{c_s^2} \frac{\partial \vec{\omega}}{\partial t^2} \quad (1.8)$$

$$c_s = \sqrt{\frac{\mu}{\rho}} \quad (1.9)$$

Often linear elastic material parameters are provided in terms of Young's modulus E and Poisson's ratio ν . They are related to the Lamé parameters λ and μ by,

$$\lambda = \frac{\nu E}{(1 + \nu)(1 - 2\nu)} \quad (1.10)$$

and

$$\mu = \frac{E}{2(1 + \nu)} \quad (1.11)$$

Often the material parameters bulkmodulus B and shear modulus G are used also. They can be written as,

$$B = \lambda + \frac{2}{3}\mu \text{ and } G = \mu \quad (1.12)$$

Elementary solution for 1D wave equation

A general solution of the 1D wave equation for P-waves will be derived using elementary theory. This theory supposes that the motion due to the wave is primarily one dimensional. In a linear elastic material this can be accomplished by setting Poisson's ratio ν to zero. The Lamé parameters then become $\lambda = 0$ and $\mu = \frac{E}{2}$. Substituting this in the three dimensional wave equation(1.5) and accounting for one dimensional motion by $\vec{u} = u$, gives the one dimensional wave equation,

$$\frac{\partial^2 u}{\partial x^2} - \frac{\rho}{E} \frac{\partial^2 u}{\partial t^2} \equiv \frac{\partial^2 u}{\partial x^2} - \frac{1}{c_0^2} \frac{\partial^2 u}{\partial t^2} = 0 \quad (1.13)$$

were $c_0 = \sqrt{\frac{E}{\rho}}$ is the phase velocity of the one-dimensional wave.

It can be shown that the d'Alembert solution fullfills the equation (see e.g.[1]). It is often written as,

$$u = f_1(k(x - c_0 t)) + f_2(k(x + c_0 t)) \quad (1.14)$$

where f_1 and f_2 are arbitrary, twice-differentiable functions and $k = \frac{2\pi}{\lambda}$ is termed the wavenumber. It can be seen that f_1 describes a wave propagating in positive x direction and f_2 one propagating in negative x direction.

In this report the case will be considered were we have a slender beam of infinite length, loaded with a prescribed strain history at it's edge. This boundary condition can be written as,

$$\varepsilon_{BC}(t) = \varepsilon(x=0, t) \quad (1.15)$$

For this reason we want a solution in terms of strains instead of displacements. This can be achieved by taking the partial derivative of the one-dimensional wave equation(1.13) with respect to x ,

$$\frac{\partial^2}{\partial t^2} \left(\frac{\partial u}{\partial x} \right) = c_0^2 \frac{\partial^2}{\partial x^2} \left(\frac{\partial u}{\partial x} \right) \quad (1.16)$$

This equation shows that the strain $\partial u/\partial x$ is governed by the same one-dimensional wave equation that governs the displacement. Since the beam is defined for positive x values only and since the boundary condition is applied at $x = 0$ the only physical realistic wave will be a forward propagating one. The general solution now will be of the form,

$$\frac{\partial u}{\partial x} = f(k(x - c_0 t)) \quad (1.17)$$

Applying boundary condition (1.15) and knowing that in a one-dimensional linear elastic material there will be no dispersion, the analytical solution for the strain history inside the slender beam becomes,

$$\frac{\partial u(x, t)}{\partial x} = \varepsilon_{BC}(k(x - c_0 t)) \quad (1.18)$$

with $\frac{2\pi}{T} = kc_0 \equiv \omega$ i.e. the circular frequency of the wave.

Chapter 2

Numerical simulation of elastic wave propagation: theoretical considerations

When performing numerical simulations two phenomena are of importance. Firstly the accuracy of the computation and secondly the numerical stability. These phenomena are influenced by both spatial and temporal discretisation used in Finite Element models (FE). The presence of these effects within FE-codes commonly used for modelling head impacts, will be investigated using results of analytical analysis. In this report the FE code MADYMO will be used as reference code but it's characteristics are common to many packages used for head impact modelling.

2.1 Numerical stability

In most FE packages used for head modelling time discretisation is performed using explicit time integration methods such as the Central Difference method (e.g. LS-DYNA3D, PAM-CRASH, Abaqus-explicit). In such explicit time schemes no iteration is performed during one time increment, providing low computational effort per time step. However, the maximum time step size that can be used is limited since explicit integration schemes are conditionally stable (i.e. stable for a time step below a certain value). The maximum size of the time step Δt_{max} is determined by the Courant number [4], defined as,

$$C = \frac{c \cdot \Delta t_{max}}{\Delta x} \leq 1 \quad (2.1)$$

In words this requirement means that the time step used should be such that during one time step the traveling distance of the fastest wave in the model ($c \cdot \Delta t_{max}$) should be smaller than the smallest typical element size in the mesh (Δx). Usually this stability requirement gives an upperbound for the timestep to be used. If a smaller time step is taken the integration procedure will be more accurate in general.

2.2 Numerical accuracy

When computing wave propagation using FE-modelling, two main error sources can be distinguished: *numerical dispersion* and *spurious reflections*. Both error sources are mainly influenced by the spatial discretisation (i.e. element formulation and mesh density) used. For this reason results of so called semi-discretisation analysis will be presented in which only spatial discretisation is accounted for.

MADYMO achieves spatial discretisation by using constant stress elements with lumped mass matrices. These contain eight integration points when full integration is applied. A reduction of computational costs can be achieved by using a reduced integration technique in which only one integration point per element is used. As a result numerical induced (i.e. artificial) zero energy modes, or hourglass modes, may occur. This can be prevented by adding an additional, non-physical, damping or stiffness, the so called hourglass parameter.

Numerical dispersion

Numerical dispersion is the phenomenon that waves of different wavelength travel at different phase velocities through the medium due to numerical artifacts. Belytschko and Mullen [2] analytically investigated semidiscretisation errors in one-dimensional cases. They found that, for constant strain elements with lumped mass matrices, the phase velocity in the discrete mesh c_{FEM} can be related to the theoretical phase velocity c by

$$\frac{c_{FEM}}{c} = \frac{\sin\left(\frac{\pi\Delta x}{\lambda}\right)}{\frac{\pi\Delta x}{\lambda}} \quad (2.2)$$

This means that the phase velocity in the discrete mesh is dependent on the wavelength λ and element size Δx . Also it can be seen that there cannot be any wave propagation when $\Delta x = \lambda$. Since wavelength λ is related to its frequency f by the phase velocity c , an upperbound on the frequency in the mesh for which no waves will be propagated can be found as,[2][6]

$$f_{cutoff} = \frac{c}{\Delta x} \quad (2.3)$$

Mullen and Belytschko [10] extended this analysis to two dimensional finite element semi-discretisations. Since they considered the two dimensional wave equation, this means that the analysis holds for both P-waves and S-waves. Figure(2.1) shows the effect of the angle of the normal of the incident wave front with the mesh, Θ , on dispersion $\frac{c_{FEM}}{c}$ in square elements. Both full and reduced integrated elements were investigated. The results show that for $\Theta = 0$, no

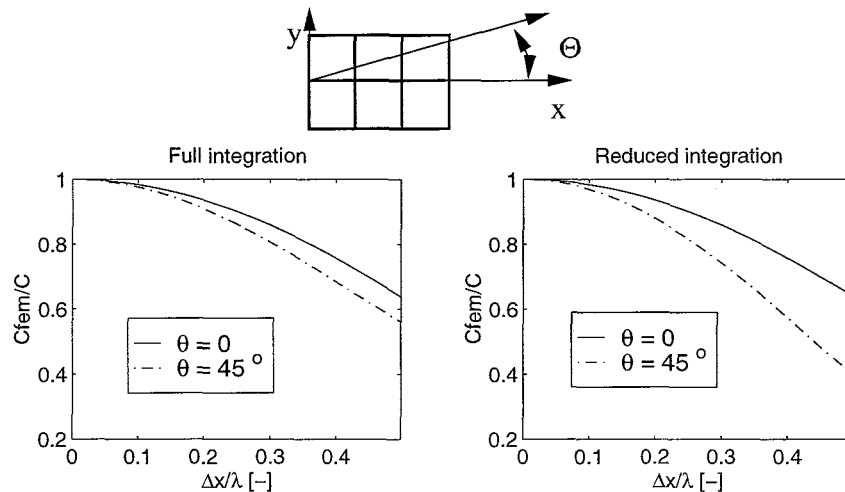


Figure 2.1: Dispersion of bilinear quadrilateral elements with lumped mass, as a function of relative mesh density $\frac{\Delta x}{\lambda}$ for various directions Θ (extreme values shown).

differences between fully and reduced integrated elements exist. When a wave arrives at a certain angle $\Theta \neq 0$, the dispersive errors in the reduced integrated elements increase stronger than in the fully integrated ones.

Spurious reflection due to mesh nonuniformity

In a uniform finite element mesh, elastic waves propagate without reflection. However, due to nonuniformity in the mesh distribution, spurious reflections can occur in the computed solution. Bažant *et al.* [6] analyzed a compressive wave traveling in a rectangular mesh consisting of two uniform parts with different element sizes (h and H in Figure 2.2). Amplitudes of the waves diffracted and reflected at the transition plane between the mesh parts were analytically derived. Influences of mesh size ratio $\frac{H}{h}$, and number of elements per wave length of the second mesh part ($\frac{\lambda}{H}$) were determined. In Figure(2.3) the amplitudes of diffracted and reflected waves are provided

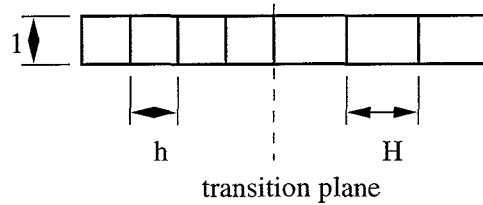


Figure 2.2: Rectangular Finite Element Mesh used by Bažant *et al.* [6].

as function of mesh size ratio $\frac{H}{h}$ and relative mesh size $\frac{\lambda}{H}$. Both are normalized to the amplitude of the incident wave. In the ideal case it would be expected that the amplitude of the reflected wave would be zero whereas the amplitude of the, normalized, diffracted wave would be equal to one.

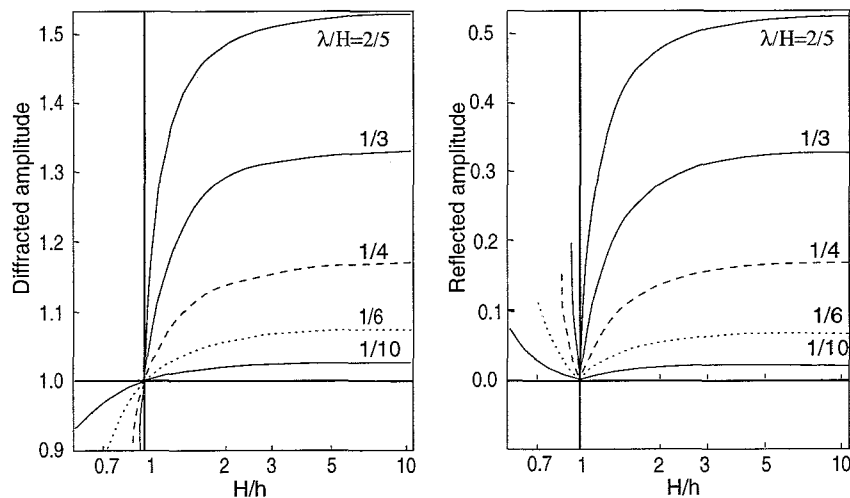


Figure 2.3: Amplitude of diffracted wave and reflected wave normalized to 1, as function of mesh size ratio $\frac{H}{h}$ and relative mesh size $\frac{\lambda}{H}$. (Copied from [6])

Figure(2.3) shows spurious reflection when a wave passes between two elements of different sizes. It can also be seen that this effect is more prominent when wave length λ covers only a few finite element sizes H . If $\lambda = 10H$ the amplitude of the reflected wave still equals 2.5% of the amplitude of the incident wave for mesh size ratios of 2 and more. When a wave travels from a coarser mesh to a more refined mesh (mesh size ratio, $\frac{H}{h} < 1$), the error seems to grow much faster than in the case that $\frac{H}{h} > 1$. Although not mentioned by the authors, this asymmetric behaviour is probably due to the fact that the curves are determined for constant relative mesh size parameter $\frac{\lambda}{H}$. Whereas the accuracy of the mesh is in general determined by the coarsest mesh. For this reason the error when $\frac{H}{h} < 1$ has to be based on the accuracy measure $\frac{\lambda}{h}$ instead of $\frac{\lambda}{H}$. A simple analysis for $\frac{H}{h} = \frac{1}{0.7}$ proved that the error induced by a transition from a coarse

mesh to a fine one is the same as the other way around¹. However, these findings have not yet been validated for more than one mesh size ratio.

2.3 Implications for existing head models

In the quest for establishing insight in the development of injury during an impact of the head, Finite Element head models are used to assess the dynamical behaviour of the head. A potential cause for the appearance of head injury is the focussing effect of compressive and shear waves traveling through the brain tissue. Most FE models found in literature consist of constant strain elements with an average element size $\Delta x = 1.0 \cdot 10^{-2} m$ (e.g. [7][8]). Since nearly incompressible brain tissue has to be modelled, full integrated elements may show locking phenomena (i.e. strong overestimating of element stiffness). For this reason reduced integrated elements are often used.

Linear (visco)elastic material behaviour for the brain tissue is often assumed, for this reason the theory of previous section can be used to assess if current headmodels are capable of describing wave phenomena correctly.

Numerical dispersion

As shown in Figure(2.1) the dispersive behaviour depends on the direction Θ by which waves are arriving on a mesh. Let's consider the worst case scenario: $\Theta = 45^\circ$. If we want the maximum error to be less than 1% (i.e. $\frac{c_{FEM}}{c_0} = 0.99$), we find that $\frac{\lambda}{\Delta x_{red}} = 17.7$ for reduced integrated elements. This relation and the estimated $\Delta x = 1.0 \cdot 10^{-2} m$ provide the smallest wavelength that can be computed correctly $\lambda_{min} = 17.7 \cdot 10^{-2} m$.

The maximum frequency that can be computed correctly can be determined using,

$$f_{max} = \frac{c}{\lambda_{min}} \quad (2.4)$$

- P-waves travel through the brain tissue at approximately $1500 \frac{m}{s}$ [3], so the maximum frequency equals $8.5 \cdot 10^3 Hz$.
- S-waves travel at approximately $5 \frac{m}{s}$ ($1 \cdot 10 \frac{m}{s}$ [9]) yielding a maximum frequency of $28 Hz$.

Spurious reflection

From figure(2.3) it can be concluded that for reducing the change of amplitude of a wave traveling through a nonuniform mesh to less than 2.5 % the mesh distribution has to such that $\frac{\lambda}{\Delta x} \geq 10$. Since this is already achieved by fulfilling the requirements with respect to dispersion, spurious reflections should be low. However, it has to be reminded that the spurious reflection analysis was primarily one dimensional and that effects of different element shapes were not included.

2.4 Methods of improvement

Until now the effects of spatial discretisation as it is implemented in MADYMO have been taken into account. Nothing has been said on effects of time-discretisation and on different spatial

¹Example: For comparing the spurious reflection when $\frac{H}{h} = 0.7$ with the the one when $\frac{H}{h} = \frac{1}{0.7}$ for a given relative mesh size $\frac{\lambda}{\Delta x_{max}} = 4$ the following approach has to be followed,

1. For $\frac{H}{h} = \frac{1}{0.7}$ the relevant relative mesh size $\frac{\lambda}{\Delta x_{max}} = \frac{\lambda}{H} = 4$. Figure(2.3) shows that the amplitude of the diffracted wave, $|\gamma|$, increases by approximately 10%.
2. For $\frac{H}{h} = 0.7$ the relative mesh size is determined by h and equals $\frac{\lambda}{h} = 4$. Using $\frac{\lambda}{H} = \frac{h}{H} \frac{\lambda}{h}$ it can be determined that $\frac{\lambda}{H} = \frac{4}{0.7} = 5.7$. Reading the error at this curve gives a decrease of amplitude $|\gamma|$ by approximately 10%.

This analysis also holds for the reflected spurious wave.

discretisation methods. A few comments on the use of these methods will be given using the findings of the authors referenced already.

1D dispersion

Until now only elements with diagonalized (lumped) mass matrix were considered. Lumped mass matrix are known to be computationally more effective but do not allow a very accurate frequency representation. Belytschko et al. [2] also investigated elements with a generalized mass matrix obtained by using a weighting factor α by,

$$M = \alpha M_{consistent} + (1 - \alpha) M_{lumped}$$

It was concluded that elements with consistent mass matrix tend to overestimate wave velocities whereas the ones with lumped mass matrix underestimate the wave velocity. The least dispersion was obtained when α was set to $\frac{1}{2}$.

When time integration is applied by using the Central-Difference integration scheme, the dispersive behaviour of lumped mass elements can be improved if the timestep is chosen close to the critical timestep determined by the Courant number (equation(2.1)).

Elements with quadratic interpolation functions were found to display a negligible dispersion behaviour. However these elements can introduce a significant amount of additional noise into the solutions due to the existence of two solutions at each wavelength (for more information please refer to Belytschko et al. (1977)[2]).

2D dispersion

Mullen *et al.* found that quadrilateral elements with a consistent mass matrix show the best performance[10]. Mass lumping decreases the performance, particularly in directions that don't coincide with the mesh lines. This is further exacerbated by reduced integration.

Spurious reflections

As far spurious reflections are concerned, the consistent mass is superior to the lumped mass matrix, giving about one-half of the amplitude of the reflected wave[6]. Investigating the time integration showed that this has no effects on the reflective behaviour.

It can be concluded that there is not an optimal method for modelling wave propagation. A method to prevent spurious wave reflection as well as wave dispersion from overshadowing the true dynamic response is to eliminate all wavelengths which are smaller than the critical wavelength determined using equation(2.2) or Figure(2.1). This can be done by expanding the applied load in a Fourier series and delete all frequency terms corresponding to wavelengths smaller than the critical one [6]. An other possibility is to adjust the mesh size such that the greatest part of the frequency contents of the applied load can be modelled correctly.

2.5 Conclusions

Simulation of wave phenomena with the Finite Element Method introduces numerical artifacts, dispersion and spurious reflection. It can be derived analytically that these errors increase with increasing element size. From a two dimensional dispersion analysis it can be concluded that for constant strain elements, with lumped mass matrix the choice, $\Delta x = \frac{1}{18} \lambda$ leads to an error in wave propagation velocity of approximately 1 %. Applying the same relative mesh size in non-uniform meshes gives a reflected wave with an amplitude of 2.5 % of the incident wave amplitude.

In current FE-head models the element size is typically 0.01 *m*. This means that the wave length that can be described accurately is about 0.18 *m* which corresponds to the typical size of a 50th percentile head (anterior - posterior head size, 0.195 *m*, head width, 0.155 *m*[15]). From this

it can be concluded it is very unlikely that that wave propagation can be described accurately in current headmodels.

Chapter 3

Numerical simulation of elastic wave propagation: MADYMO computation

In this chapter, it is investigated whether the MADYMO-solutions of wave propagation problems behave as predicted theoretically in the previous chapter. For this reason the propagation of one dimensional P-waves in a slender linear elastic beam is investigated. Since MADYMO uses three dimensional geometry, one dimensional conditions are obtained by setting Poisson's ratio to zero. The beam is excited by applying a force history on one edge. The theory of the previous chapter will be applied to determine the correct mesh density and computed results will be compared with the analytical solution.

3.1 Analytical solution of the 1D wave equation

The beam is loaded by a prescribed force history at one edge. Nahum et al. [11] obtained this pulse by impacting a head of a seated cadaver. It is often used for a benchmarking head models (e.g. [7][8]). For reasons of simplicity this pulse is approximated by,

$$F(t) = F_{max} \sin^4(2\pi ft) \quad (3.1)$$

with $F_{max} = 6900 N$ and $f = 62.5 Hz$ (see also Figure(3.1)). Since there is only one dimensional motion, the cross-area of the beam remains constant ($A = A_0$). For this reason the prescribed force can easily be written as a prescribed strain using, $\varepsilon(t) = \frac{F(t)}{EA_0}$. Substituting this in the general one dimensional solution for a wave traveling in positive x-direction (equation(1.17)) and using $\kappa = \frac{2\pi f}{c_0}$, the analytical solution for the strain becomes,

$$\varepsilon(x, t) = \frac{F_{max}}{EA_0} \sin^4\left(\frac{2\pi f}{c_0}(x - c_0 t)\right) \quad (3.2)$$

The material properties of the beam are chosen such that the one-dimensional wave propagation velocity c_0 approximates the speed of sound in brain tissue ($1500 \frac{m}{s}$ [3],[12]). They are shown in Table 3.1. The length of the beam was chosen to be such that no reflection on the outer edge would occur during the simulation.

3.2 The numerical model

A beam with square cross-section has been modelled using cubic elements, with one element per cross-section of the beam. The length of the beam was chosen to be such that no reflection on the

Table 3.1: Material parameters for linear elastic slender beam.

Material parameter	Value
E	$2.25 \cdot 10^9$ [Pa]
ν	0.0 [-]
ρ	1000 [kg/m ³]
$c_0 = \sqrt{\frac{E}{\rho}}$	1500 [m/s]

outer edge would occur during the simulation. The impact on the beam has been modelled by a prescribed nodal force on the nodes at the beam edge at $x = 0$.

3.2.1 Discretisation requirements

As can be concluded from chapter 2, choices of both spatial and temporal discretisation depend on the wave length we expect in the mesh. Since a linear elastic material model is used, the frequencies in the input force are the same as in the resulting strain waves so the wave length can be determined directly from the frequencies using $f = \frac{c_0}{\lambda}$. A problem in this is that in a real input pulse more than one frequency is present. For this reason a maximum relevant frequency will be defined on which the mesh density will be based. A parametric study will provide insight whether this choice was correct.

Impact conditions

For obtaining the relevant frequency contents of the input pulse, the power spectral density (PSD) of the force signal has been determined. Such PSD shows the power contents per frequency present in the pulse. For correct modelling of the wave propagation it is assumed that we need 99 percent of the total power contents of the input. This can be obtained by integrating the PSD over frequency (using the trapezoidal method) until we reach the frequency at which the total power reaches 99% of the maximum power (as illustrated in Figure(3.1)). The maximum relevant frequency then becomes $f_{max} = 3750$ Hz.

Spatial discretisation

The wave velocity c_0 , from Table 3.1, and the maximum relevant frequency of the input force, $f_{max} = 3750$ Hz, give us the smallest wavelength that has to be described correctly, $\lambda_{min} = \frac{c_0}{f_{max}} = 0.40$ m. Since this is a one dimensional wave propagation problem we assume that the 1-D dispersion relation of equation(2.2) is valid. When an accuracy of 1% is required (i.e. $c_p/c_0 = 0.99$) this yields a maximum element size $\Delta x = 3.12 \cdot 10^{-2}$ [m]. It has been chosen to split the beam into 1000 quadrilateral elements, with element length $\Delta x = 3.0 \cdot 10^{-2}$ [m].

Temporal discretisation

The maximum timestep required for stability is determined by the Courant number defined by equation(2.1). Setting the Courant number to one using $\Delta x = 3.0 \cdot 10^{-2}$ [m] yields the maximum timestep, $\Delta t \leq 2.0 \cdot 10^{-5}$ [s]. This is small enough to describe the maximum relevant frequency in the input force.

Since both spatial discretisation and time integration influence the accuracy, the Courant number of the mesh used is set to $\frac{1}{2}$ for all simulations unless stated differently. This provides the time step, $\Delta t = 1 \cdot 10^{-5}$ [s]. The simulation time has been set to 20 [ms], which is the theoretical time for the wave to reach to end of the beam.

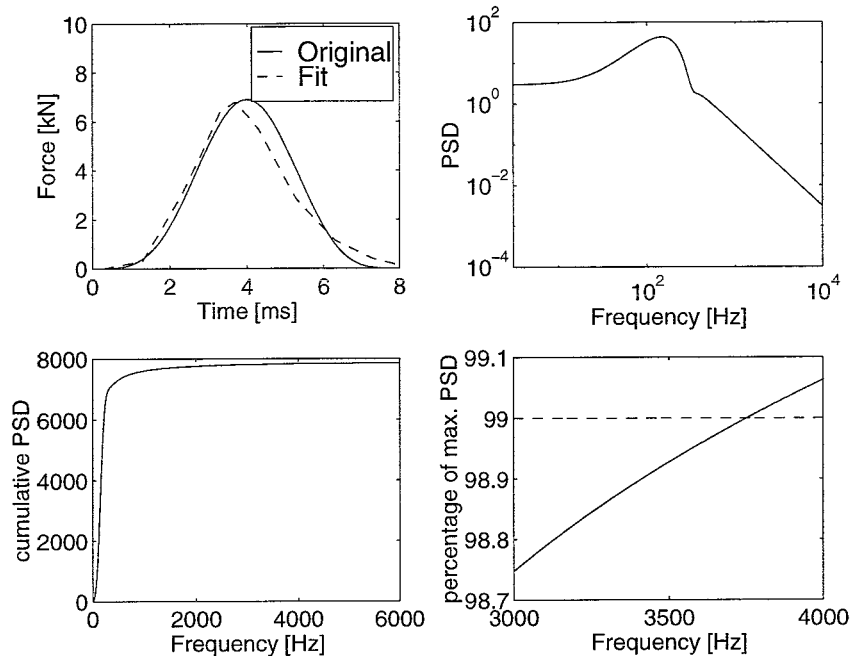


Figure 3.1: Input force history and power spectral density fitted on Nahum pulse [11].

3.3 Results

In Figure(3.2) both analytical and numerical strain values in the beam are shown as contour lines in the time-x-coordinate, domain. To illustrate how to interpret such contour plot, two cross-sections are also provided in this figure. The wave propagation velocity can be determined from the contour plots by taking the tangent at of each contour line of constant strain (see e.g. [1]). The wave propagation velocity has been determined out of twelve contour lines at six strain values ($\varepsilon \cdot 1000 = -1.0, -1.5, -2.0, -2.5 - 3.0 [-]$). This yields a wave velocity of 1501.3 m/s , with variance of 0.43 m/s , an overestimation of approximately 0.1%. The maximum relative strain error has been computed as the difference between numerical and analytical strain values, normalized with respect to the maximum theoretical strain value. This error starts very small and grows as the wave travels along the beam. The maximum value therefore will be reaches at the end of the simulation and equals about 1.0 %.

3.4 Parametric study

Dispersion: Spatial discretisation

To investigate when dispersion errors become of importance, calculations with coarser meshes have been carried out. In changing the mesh density, care has been taken to keep the initial elementshape cubic. This has been obtained by increasing the area of the beams edge and by altering the prescribed load such that the applied stress stays the same for all mesh densities. Also the time step has been adapted such that for each mesh the Courant number remains $\frac{1}{2}$. The maximum relative error as well as the wave velocities have been determined for each mesh density. Both data are shown in Figure(3.3).

Increasing the mesh size provides lower wave propagation velocities, as expected theoretically. Figure(3.3) shows that for mesh sizes larger than 0.74 [m] the mean dispersion error becomes larger than 1%. Velocity values determined at increasing absolute strain values, at the wave front, are smaller than the ones determined at decreasing strain values after passage of the wave (indicated

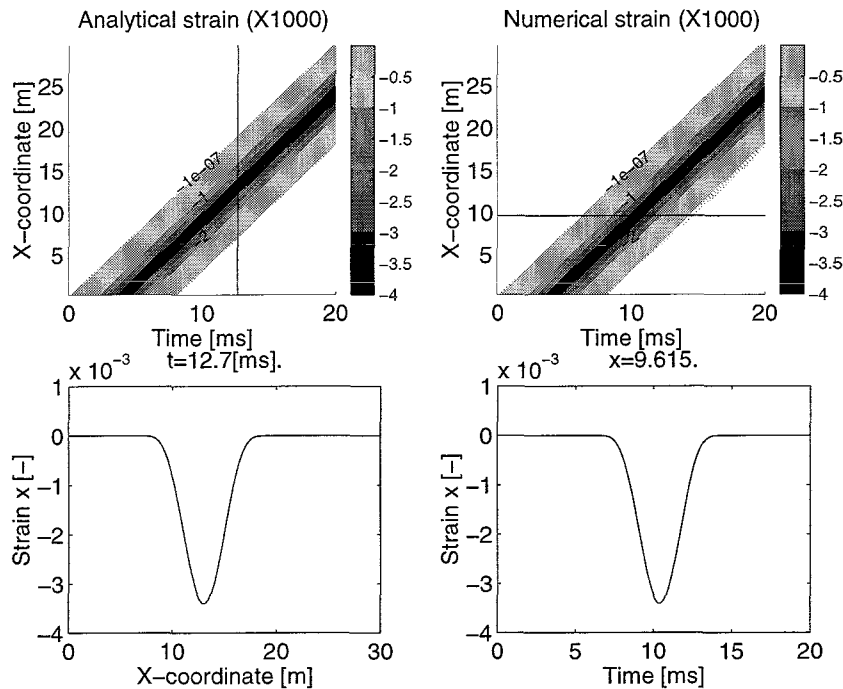


Figure 3.2: Characteristics of several strain values in x-direction. (topleft: analytical solution, topright: numerical solution ($dx = 0.03 m$)). Cross-sections at constant time and x-coordinate provided for clarification (bottom left and right respectively). Both numerical and analytical solutions printed in each cross-section.

by the maximum and minimum strain values in Figure(3.3)). This dispersion effect is larger for coarser meshes. It is caused by the fact that the input pulse contains more than one frequency. This causes the resulting wave shape in the beam to be a wave envelope, i.e. a combination of waves with different wavelengths. Dispersion theory states that waves with long wavelengths travel faster in a mesh than short ones (see Figure(2.1)). As a result the wavelength distribution in the wave envelope will change during traveling along the beam. Components with short wave lengths will travel with a velocity below the average envelope velocity defining the rear /of the wave. Components with long wavelengths will move with a velocity greater than the average envelope velocity, defining the wavefront.

Figure(3.3) shows that the maximum relative error is more or less a constant at approximately 1% for mesh sizes smaller up to $0.24 m$. For coarser meshes the error increases dramatically. For mesh size $dx = 0.74 m$, at which the mean dispersion error equals 1.0%, the maximum relative error reaches approximately 10.0 %. The use of fully integrated elements instead of reduced integrated elements did not change the error, as was expected from theory by Belytschko et al. [2].

Dispersion: Temporal discretisation

The effect of time step size is investigated by comparing results obtained using the Courant numbers 0.8475^1 and 0.5 . Again the wave velocity is determined over ten contour lines at five constant strain values. Mean values, maxima and minima are plotted in Figure(3.4).

It can be seen that decreasing the time step size leads to an increasing dispersion error. This is due to the fact that the error introduced by the Central Difference Time Integration scheme used by MADYMO is compensatory with the dispersion error caused by the spatial discretisation. It can be derived theoretically, that for a Courant number $C = 1$ no dispersion will occur when

¹This is the maximum Courant number MADYMO allows.

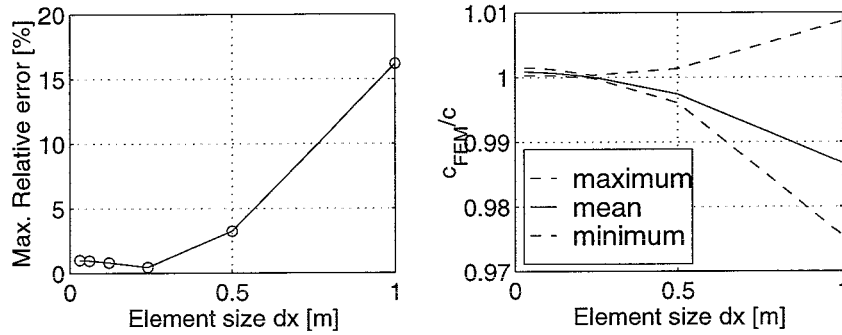


Figure 3.3: Effect of mesh density on maximum relative strain error (left) and on dispersion behaviour (right). Maximum and minimum velocities provided for range indication.

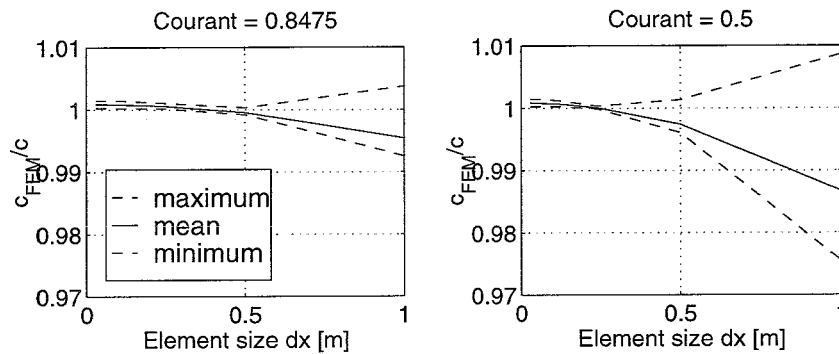


Figure 3.4: Effect of time step variation on dispersion. Mean, maximum and minimum values provided for range indication.

elements with linear displacement interpolation functions are used [2].

Spurious reflection

For this analysis the same numerical layout has been used as in the analytical analysis by Bažant et al. [6]. Only now, three dimensional elements were used instead of two dimensional ones. The mesh is shown in Figure(3.5). In chapter 2 it is shown that significant spurious reflection occurs

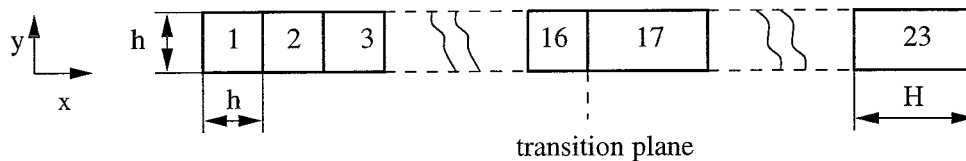


Figure 3.5: Schematic side view of the mesh used for spurious reflection analysis.

when the ratio $\frac{\lambda}{H} = 6$. Due to the fact that the input signal contains more than one frequency, it proved to be impossible to determine which λ had to be chosen as minimum wavelength in the mesh. For this reason λ is estimated to be the largest wavelength in the theoretical wave equation, i.e. $\lambda_{max} = \frac{c}{2f_{min}}$ With $f_{min} = 62.5$ [Hz] (equation(3.2)). This yields $\lambda_{max} = 12m$ and $H = 2m$. The ratio $\frac{H}{h}$ is chosen to be two. The transition between the mesh densities is positioned at $x = 16m$. Figure(3.6) shows the strain results of both homogeneous meshes as well as the non homogeneous one. The time step is chosen the same for all simulations shown. Two phenomena can be observed in this figure. A spurious wave can be observed in the nonuniform

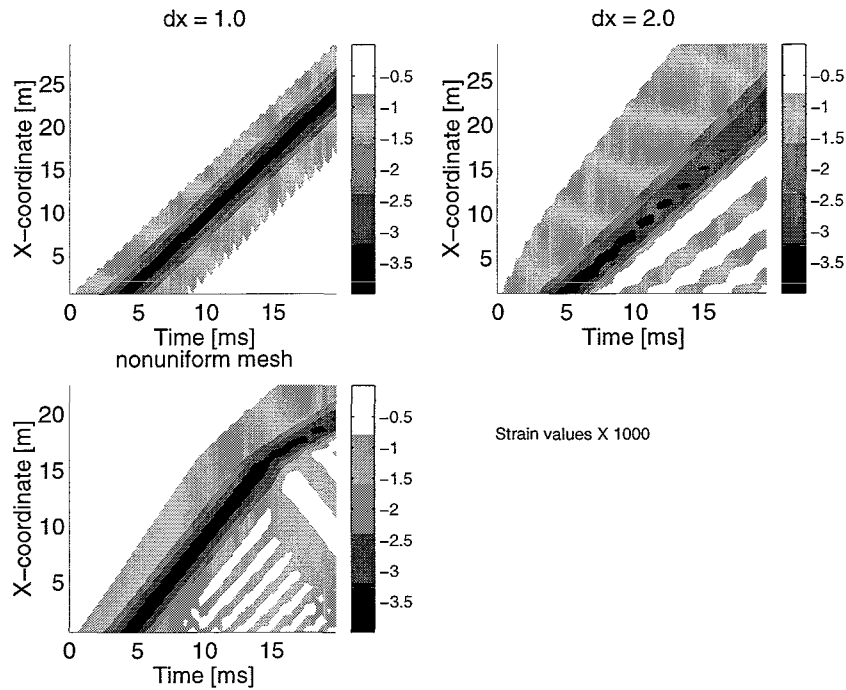


Figure 3.6: Spurious reflection due to mesh nonuniformity. Strains of mesh uniform meshes shown as well as nonuniform one (bottom left). All simulations performed using the same time step.

mesh (gray-white lines with negative slope in lower left figure). However the amplitude of this wave is of the same order than the dispersion errors. Also it can be seen that the velocity of the wave propagating in positive x -direction after the transition is lower than before the transition. This difference is not caused by dispersion, since the wave velocity for the coarsest mesh (slope of contours in top right figure) is larger than the slope seen in the nonuniform result.

3.5 Conclusions and discussion

For modelling wave propagation correctly it is assumed the maximum error in wave velocity due to numerical dispersion has to be less than 1%. Dispersion theory on one dimensional wave propagation shows that this can be obtained by using 13 elements per wavelength (refer to equation(2.2), on page 12). This is valid for both P- and S-waves consisting of one wavelength only. In reality more than one frequency is present in an input pulse. As a result a wave envelope. i.e. an assembly of waves with different wavelengths, will develop in the beam. For this reason it is not obvious on which wavelength the mesh size has to be based. Investigating this by varying the mesh density revealed that 1.0% underestimation of the wave velocity occurs at an element size $\Delta x = 0.75 m$. A rule of thumb for determining the correct mesh density at this input pulse now can be given by relating this mesh size to the largest wavelength we expect in the mesh, λ_{max} . With $T_0 = 8 ms$, the duration of the input force, and wave velocity $c_P = 1500 m/s$, we obtain that the maximum wavelength will be, $\lambda_{P,max} = c_P \cdot T_0 = 12 m$. It can be concluded that 16 elements per maximum wavelength are required for modelling this pulse.

The theory on the accuracy of FE modelling presented in chapter 2, is valid for both P- and S-waves. For this reason we assume that for modelling waves in MADYMO with a certain accuracy, the number of elements per wavelength is the same for both S-waves and P-waves. If the same input pulse is used for generating a shear wave, the mesh size needed for accurately modelling the resulting wave envelope follows from $\Delta x_S = \frac{c_S \cdot T_0}{16}$. Applying the shear wave velocity $c_S = 5 m/s$,

gives a mesh size of $\Delta x_S = 2.5 \cdot 10^{-3} m$.

For judging if the required dispersion accuracy of 99% is realistic, the maximum strain errors normalised with the maximum occurring strain value will be analysed. At the required 99% dispersion accuracy, the maximum relative error equals approximately 10% when the P-wave has travelled 30 m inside the beam, i.e. when the wave has traveled 40 element lengths. If S-waves are modelled using the same dispersion accuracy, the error will also be 10% at 40 element lengths. The mesh size for modeling S-waves at this accuracy equals $2.5 \cdot 10^{-3} m$ so the distance at which a relative strain error for S-waves reaches 10% equals 0.1 m .

Numerical dispersion does not only influence the mean velocity of the wave envelope, it also changes the shape of the envelope, waves with long wavelengths will travel faster in a mesh than short ones. For this reason the wave velocities calculated at increasing strain values (i.e. at arrival of the strain wave) are higher than the ones calculated at strain values when the strain decreases.

The presence of spurious reflection at the transition between two mesh densities occurred at low mesh densities only at which dispersion effects overrule the spurious reflection effects. For this reason a quantitative error investigation could not be performed. It was observed that there was also a change in wave propagation velocity after the wave passed the transition. This change does not correspond with the difference in propagation velocities of the uniform meshes separately. Nevertheless it can be concluded that for the one dimensional situation, spurious reflections will not be significantly important when the mesh is chosen such that dispersion error is low (e.g. less than 1%).

Chapter 4

Importance of wave phenomena in the human head

After having considered general wave theory in chapter 1 and numerical aspects in chapters 2 and 3, it will be estimated in this chapter to which extent wave phenomena are present in the human head during an impact. This estimate will be based on required boundary conditions, damping and reflection behaviour.

4.1 Boundary conditions for wave propagation

P-waves and S-waves exist at different frequencies due to their different propagation velocities. A lower bound for the frequency range for each type of wave can be found by considering the largest wave that fits within the head. P-waves and S-waves exist at different frequencies due to their different propagation speeds. The lowest frequency for a wave to exist in the head can be estimated by,

$$\lambda_{max} = \frac{c}{f_{min}} \leq D_{head} \quad (4.1)$$

where D_{head} represents a typical measure for the diameter of the head. Assuming a head diameter of 0.2 m and applying a shear wave velocity of 5 m/s gives that the lowest frequency equals 25 Hz for S-waves. For P-waves the propagation velocity is 1550 m/s , providing a minimum frequency of 7750 Hz .

4.2 Effect of damping

An upperbound of the frequency range of the two wave types can be found by accounting that brain tissue behaves like a visco elastic solid. In this analysis it is assumed that linear visco elastic material behaviour is valid. The amplitude decay of plane waves is determined as function of frequency and distance traveled. Plane waves are well suited for estimating the effect of visco elasticity since they do not show amplitude decay when viscous behaviour is absent. Furthermore we consider harmonic waves. This is allowed since a transient wave can be thought of as a contribution of a number of time harmonic waves. It will be assumed that steady state has been reached. The theory presented will be a summary of what can be found in, [16] sections 10.4 and 10.5.

The general solution for a forward propagating time-harmonic displacement wave can be written in complex notation as,

$$\vec{u} = A\vec{d}e^{i(k(\omega)\vec{x}\cdot\vec{p}-\omega t)} \quad (4.2)$$

were ω is the angular frequency, $k(\omega)$ the wave number and \vec{p} and \vec{d} are unit vectors in the directions of propagation and displacement respectively. For linear visco elastic material behaviour the wave number $k(\omega)$ is a complex number, with real part $k_r = Re(k(\omega))$ and imaginary part $k_i = Im(k(\omega))$. As a result the solution will be of the form,

$$\vec{u} = A\vec{d}e^{-k_i\vec{x}\cdot\vec{p}}e^{i(k_r\vec{x}\cdot\vec{p}-\omega t)} \quad (4.3)$$

It shows that the amplitude of the wave decreases as function of the imaginary part of the wavenumber and the distance traveled $\vec{x}\cdot\vec{d}$. For P-waves ($\vec{d} = \pm\vec{p}$) the complex wave number can be written as,

$$k_p = \omega\sqrt{\frac{\rho}{B^*(\omega) + \frac{4}{3}G^*(\omega)}} \quad (4.4)$$

with $B^*(\omega)$ the complex bulk modulus and $G^*(\omega)$ the complex shear modulus. Both moduli can be written in the form,

$$G^*(\omega) = G'(\omega) + iG''(\omega), B^*(\omega) = B'(\omega) + B''(\omega) \quad (4.5)$$

were $G'(\omega)$ and $B'(\omega)$ are storage moduli and, $G''(\omega)$ and $B''(\omega)$ are loss moduli. When a loss modulus equals zero, the complex modulus becomes the real linear elastic modulus defined by equation(1.12) on page 8.

The complex wave number of S-waves is defined as,

$$k_s = \omega\sqrt{\frac{\rho}{G^*(\omega)}} \quad (4.6)$$

For determining the effect of viscous behaviour in brain tissue the it has been assumed that the bulkmodulus is non-viscous, i.e. $B^*(\omega) = B$. Since $B \gg \mu$, it can determined from the compressive wave velocity by neglecting μ ,

$$c_p = \sqrt{\frac{B + \frac{4}{3}\mu}{\rho}} \approx \sqrt{\frac{B}{\rho}} \quad (4.7)$$

Values for storage and loss shear modulus do depend significantly on frequency. Values at upper and lower end of the measured frequency spectrum found in literature, are used to obtain an impression of the extreme situations of material damping. They are shown in Table(4.1) together with references and the frequencies at which they were determined. A more detailed overview of the material parameters can be found in [17].

Reference	G'	G''	B	Frequency [Hz]
Peters <i>et al.</i> [18]	600	150		16
Shuck <i>et al.</i> [19]	$1.5 \cdot 10^5$	$8.0 \cdot 10^4$		400
equation(4.7)	-	-	$2.4 \cdot 10^9$	all

Table 4.1: Material parameters used for estimating the viscous behaviour of brain tissue.

Application of these material parameters in the definitions for the wavenumbers and applying the wave numbers in the visco elastic solution, equation(4.3), provides the amplitude of the wave as a function of frequency $f = \frac{\omega}{2\pi}$ and distance traveled $\vec{x}\cdot\vec{p}$.

S-waves

The normalized amplitude of S-waves as function of frequency and distance traveled, is shown in Figure(4.1). In Figure(4.2) the same data are plotted differently. In the left figure the relative amplitude is plotted after the S-wave has traveled 0.1 m, being approximately the radius of the

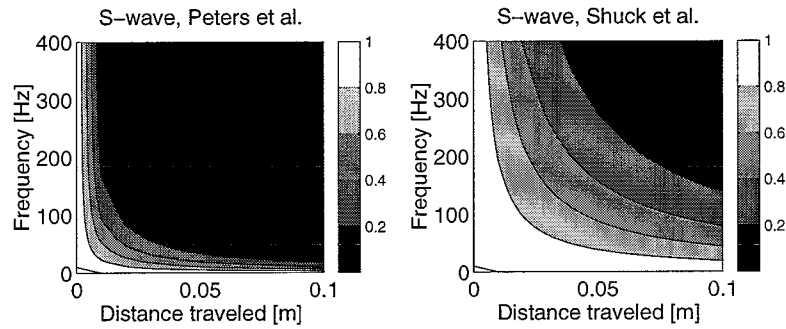


Figure 4.1: Effect of damping in brain tissue on S-waves, using linear viscoelastic theory. Amplitude normalized to one. Bulk modulus is constant. Shear moduli taken from table 4.1

human head. On the right, the distance is plotted at which half of the initial amplitude of the wave is left.

An upperbound for the relevant frequency range for S-waves in the head, can be defined as the frequency at which the amplitude of a wave remains 1% of its original amplitude, after having traveled through the head from one side to the other. By setting this distance to 0.2 m , and using the data set by Shuck et al., which is valid for the highest frequency range, an upper relevant frequency of 300 Hz can be found for S-waves.

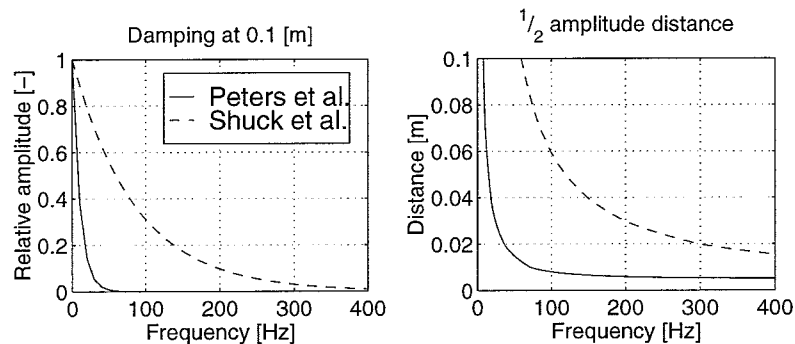


Figure 4.2: (left) Amplitude of S-wave, at distance traveled corresponding to center of brain (0.1 m). (right) distance at which amplitude of S-wave is halved versus frequency.

P-waves

Repeating the analysis performed for S-waves with the P-waves provides that the largest damping occurs when the Shuck data set is applied. The half amplitude distance then equals approximately 8.4 m at $f = 1.0 \cdot 10^6\text{ Hz}$. For this reason it can be concluded that there is no damping present for relevant pulse durations.

4.3 2D Reflection

In the analysis in the previous sections, P- and S-waves were considered separately. However, when considering the reflection behaviour this is not possible any more. In general when a wave hits a boundary of two media with different material properties, two phenomena can be observed. Firstly part of the wave will be reflected back in the and another part will be diffracted into the other medium. Secondly, waves can undergo a change of type. E.g. when a P-wave hits a

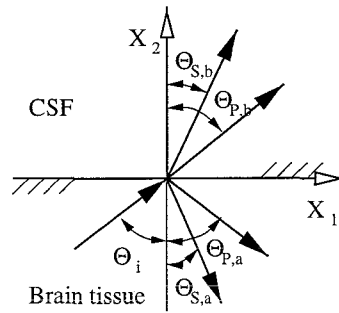


Figure 4.3: Reflected (a) and diffracted (b) P- and S-waves, due to incident P-wave (i).

boundary between two linear elastic media, four different waves will occur, a reflected P-wave, a transmitted P-wave, a reflected S-wave and a transmitted S-wave (shown in Figure(4.3)). The amplitude ratios of the different waves are determined by the material properties of both media.

In this section the reflection-refraction behaviour of compressive waves at the brain-Cerebro Spinal Fluid (CSF) interface in the head is investigated. For simplification reasons it is assumed that both brain tissue and CSF behave as two joined linear elastic half spaces. Perfect contact is assumed so displacements and stresses are continuous on the interface plane. Furthermore the interface plane is assumed to be flat. Applying these assumptions in the general solution given by equation(4.2) a system of four equations for the amplitudes of reflected and diffracted waves in terms of the amplitude of the incident wave can be derived (refer to [16], page 186). This system is solved by applying the parameters shown in Table(4.2) and varying the angle Θ_i of the incident wave between 0 and 90.

Parameter	Brain tissue	CSF
Velocity of P-waves	1550 m/s, [3]	1500 m/s, sea water [20]
Velocity of S-waves	0.1 – 10 m/s, [17]	0.0 m/s
Mass density	1000 kg/m ³	1000 kg/m ³

Table 4.2: Geometrical and material parameters used in estimating reflection behaviour of P-waves in brain tissue at CSF interface.

Figure(4.4) shows the amplitude of the various waves versus the incident angle for $c_{s,brain} = 5 \frac{m}{s}$. The amplitude of the incident wave is set to one. As was to be expected, the P-wave is almost completely diffracted into the CSF for incident angles less than 60°. This is due to the almost equal acoustic impedance for compressive waves ($Z = \rho \cdot c_p$) of brain tissue and CSF. For large incident angles the amplitude of the reflected wave increases. It is interesting to notice that diffracted P-waves with angles 75° to 90° do not exist. The development of shear waves due to reflection of the P-wave is low. A maximum of 0.3 % of the amplitude of the incident wave can be seen at an incident angle of approximately 45°. The lower right figure shows that all reflected waves travel perpendicular to the surface. Figure(4.4) seems to indicate that there is also an S-wave refracting into the CSF. The angle of this reflected wave equals zero for all incident wave angles. This means that the resulting particle motion is in in plane direction of the interface plane (i.e. x_1 direction in Figure(4.3)). Furthermore perfect contact is assumed, as a result there will be particle motion at $x_2 = 0$. However this wave will not propagate, since the wave propagation velocity $c_{s,CSF}$ is set to zero. A parametric study in which $c_{s,CSF}$ was taken very close to zero showed a convergence to the solution shown indicating that the result shown is a realistic one and not merely determined by the boundary condition at the interface plane.

The effect of the large spread for the shear velocity in brain tissue on the reflection behaviour has been investigated in Figure(4.5). It shows that the maximum amplitude of the reflected shear wave equals approximately 0.7 % of the amplitude of the incident compression wave.

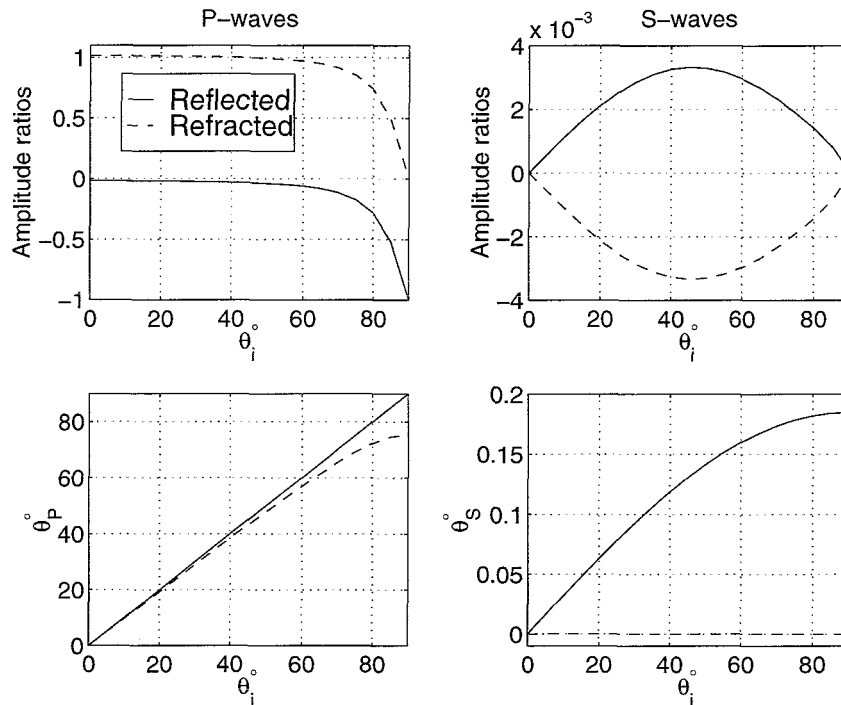


Figure 4.4: Amplitude and angles of reflected and diffracted waves, for incident P-wave with various angles θ_i . $c_{s,brain} = 5 \text{ m/s}$. Amplitude incident wave set to one. Upper figures: amplitudes normalised to incident one. Lower figures: angles of reflected and diffracted P-waves (left) and S-waves (right).

4.4 Summary and Conclusions

A simple analysis has been performed to obtain knowledge on the presence of waves in brain tissue. Both viscoelastic behaviour as well as the reflection at the brain-CSF interface has been investigated. This leads to the following conclusions.

P-waves

The minimum frequency for the existence of P-waves in the head has been estimated to be 7750 Hz . This is consistent with findings of Young and Morphey [21] who numerically analysed a fluid filled sphere and concluded that impact durations of 0.1 ms were needed to obtain a dynamic response instead of a quasi static one. At these frequencies also P-waves do not show significant damping. This can be explained by the assumption that the bulkmodulus B was elastic, i.e. real. At reflection on the brain-CSF interface, most of the P-waves was reflected into the CSF. For incident angles close to 90° the amplitude of the diffracted waves decreases while the amplitude of the reflected waves increases.

S-waves

S-wave exist from approximately 25 Hz inside a human head. The viscosity analysis showed that the maximum frequency of a wave that can be reflected in the head is approximately 300 Hz . The contribution of transition from P-waves to S-waves by reflection is low since the amplitude of the reflected shear waves was very low over the complete range of incident angles (maximum 0.7 % of the incident amplitude at an incident angle of 45°).

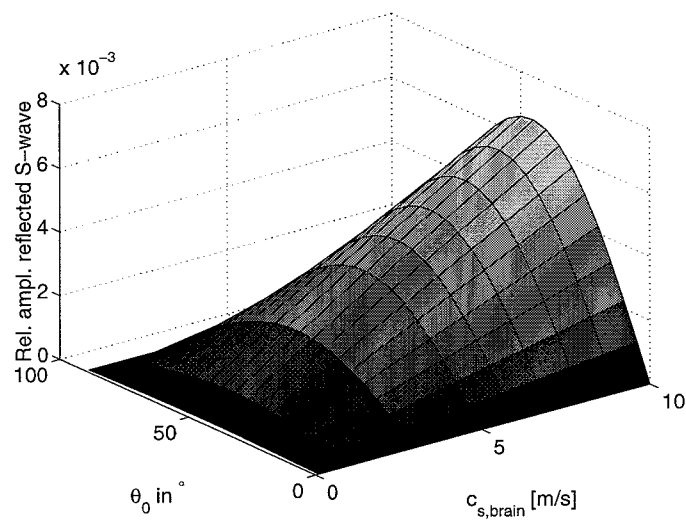


Figure 4.5: Relative amplitude of reflected shear wave as function of dilatational wave velocity in the brain tissue $c_{s,brain}$ and angle of incidence Θ_0 .

Chapter 5

Discussion and conclusions

5.1 Presence of wave propagation during head impact

The presence of certain wave types in the head depends on the impact conditions. A lower bound has been defined by considering the wavelength. A dynamic response will be called a wave phenomenon if its wave length fits inside a typical head measure (i.e. $\lambda_{max} \leq D_{head} = 0.2 m$). Dilatational or P-waves exist for $f > 7750 Hz$, while distortional or S-waves exist at $f < 25 Hz$.

The upperbound of the relevant frequency range is determined by the viscoelastic properties of brain tissue. These introduce damping which increases with frequency. For S-waves the upperbound is estimated to be $300 Hz$. For P-waves the damping is very small, for $f = 1 MHz$ the amplitude of the wave is halved after having traveled $8.4 m$. For this reason the upperbound will be determined by the excitation frequency.

From chapter 3 it can be concluded that an upperbound for the frequency in typical traffic related impacts equals $3750 Hz$. For this reason no P-waves will be present but S-waves will. In a ballistic/forensic blunt impact situation, first a direct impact with a duration of approximately 2 to $100 \mu s$ [22],[23] will occur. After this inertia will cause the head to rotate with a typical duration of order ms [24]. This means that P-waves can be present at the start and S-waves might develop later on.

5.2 Implications for accuracy of existing head models.

From theoretical analysis it can be concluded that due to the spatial semi-discretisation used in headmodelling, the wave velocity calculated will always be lower than the analytical one. When an error of less than 1% is required for the numerical wave velocity, current head models are capable of modelling compressive waves for frequencies up to $8500 Hz$ and shear waves up to $28 Hz$. For gaining insight if this is realistic the propagation of a one-dimensional P-wave in a beam has been modelled using a realistic input pulse. A P-wave has been used for obtaining a true one dimensional problem which analytically shows no dispersion. A problem was that this pulse contained more than one frequency. It was assumed that 99% of the frequency contents of the pulse had to be modelled correctly. The resulting mesh size proved to be too small, since the results were too accurate. After having established a mesh density which indeed provided a dispersion error of 1% the maximum relative strain error at the end of the beam (traveling distance equals $30 m$) became 10%. For estimating the meaning of these results for headmodelling, S-waves have to be considered since P-waves cannot exist in the head for the pulse used ($f_{max} = 3750 Hz$, refer to section 5.1). If we assume that numerical errors will be the same for S-waves as for P-waves (as theoretical expected), it can be derived that the maximum relative strain error equals 10% at a traveling distance of $0.1 m$. This is the typical head radius. This leads to the following conclusions:

- For the pulse shape used, the required dispersion error of less than 1% is a lower bound for modelling S-waves.
- Requiring the mesh to be suited for modelling 99% of the frequency contents of the input pulse is too strict. For the pulse used the critical frequency equals $\frac{5}{4T_0}$ were T_0 is the duration of the pulse.
- The mesh size needed for modelling S-waves correctly is $\frac{1}{4}$ of the mesh size currently used in headmodelling. This means that 64 times as many elements are needed.

When observing these results it should be considered that the numerical investigation is valid for the propagation of 1 dimensional P-waves only. The theory of chapter 2 shows that in the two-dimensional case, where waves do not necessarily propagate along the mesh direction, the number of elements per wavelength should be increased by 40% (Chapter 2, equation(2.2) and section 2.3). If we assume this behaviour also valid for three-dimensional numerical dispersion, 175 as much elements should be used in current three-dimensional headmodels .

Bibliography

- [1] Bedford, A. and D.S. Drumheller (1994): *Introduction to elastic wave propagation*, Wiley Publishers, Chichester, N-Y, Brisbane, Toronto, Singapore.
- [2] Belytschko, T. and R. Mullen (1977): "On Dispersive Properties of Finite Element Solutions", in *Modern Problems in Elastic Wave Propagation, Int. Union of Theoretical and Applied Mechanics*, ed by. J. Miklowitz and J.D. Achenbach, Wiley Publishers, New York, Chichester, Brisbane, Toronto, pp. 67-82.
- [3] Etoh A., Mitaku, S., Yamamoto, J. and K. Okano (1994): "Ultrasonic Absorption Anomaly of Brain Tissue", *Japanese Journal of Applied Physics*, Vol. 33, pp. 2874-2879.
- [4] Courant, R., Friedrichs, K. and H. Lewy (1928): "On the Partial Difference Equations of Mathematical Physics", *Math. Ann*, Vol.100, pp. 32-74.
- [5] TNO (1997): "MADYMO theory manual, Version 5.3", TNO-Road Vehicles Research Institute, Delft, The Netherlands, pp. 101-104.
- [6] Bažant, Z.P. (1978): "Spurious reflection of elastic waves in nonuniform finite element grids", *Computer Methods in Applied Mechanics and Engineering*, Vol. 16, pp. 91-100.
- [7] Claessens, M., Sauren, F. and J. Wismans (1997): "Modelling of the Human Head under Impact Conditions: A Parametric Study", *Proceedings of the 41th Stapp Car Crash Conference*, SEA 973338, pp. 315-328.
- [8] Kang, H-S., Willinger, R., Diaw, B.M. and B. Chinn (1997): "Validation of a 3D Anatomic Human Head Model and Replication of Head Impact in Motorcycle Accident by Finite Element Modelling", *Proceedings of the 41th Stapp Car Crash Conference*, SEA 973339, pp.329-338.
- [9] Moore, P. (1997): "A Very Smart Dummy", *New Scientist*, Vol. 2089, pp. 38-42.
- [10] Mullen R. and T. Belytschko (1982): "Dispersion analysis of finite element semidiscretizations of the two-dimensional wave equation", *Int. Journal for numerical methods in engineering*, Vol.18, pp. 11-29.
- [11] Nahum, A.M. Smith, R.W. and C.C. Ward (1977): "Intracranial pressure dynamics during head impact", *Proceedings 21th Stapp Car Crash Conference*, pp. 339-366.
- [12] Lin, S-C, Shieh, S-J and M.J. Grimm (1997): "Ultrasonic measurements of Brain tissue Properties", *Center for Disease Controll conference pre-proceedings*, pp. 27-31.
- [13] Claessens 1997: "Finite Element Modelling of the Human Head under Impact Conditions", PhD. dissertation, Eindhoven University of Technology, Eindhoven, The Netherlands.
- [14] Kolsky, H. (1963): *Stress waves in solids*, Dover Publications Inc. New York, U.S.A.
- [15] Pheasant, S. (1986): *BodySpace: anthropometry, ergonomics and design*, Taylor & Francis, London.

- [16] Aachenbach, J.D. (1973): *Wave Propagation in elastic solids*, North-Holland publishing company, London, Amsterdam, Elsevier publishing company, inc, New-York.
- [17] Brands, D.W.A. (1998): "Constitutive modelling of brain tissue (literature review)", *WFW-report 98.020*.
- [18] Peters, G. (1997): "Application of the Time Temperature Superposition Theory on Brain Tissue", *Biorheology*, Vol 34, pp 127-138.
- [19] Shuck, L. Haynes, R. and J. Fogle (1970): "Determination of Viscoelastic Properties of Human Brain Tissue", ASME Paper, No. 70-BHF-12
- [20] Kinsler, L.E., Frey, A.R., Coppens, A.B. and J.V. Sanders (1982): *Fundamentals of Acoustics*, Third Edition, John Wiley & Sons, New-York, p 462.
- [21] Young, P.G. and C.L. Morphey (1998): "Intracranial Pressure Transients caused by head impacts", *IRCOBI Conference, Göteborg*, pp. 391-403.
- [22] Booiij, S.M. (1998): "Optische weergave en kwantificatie van drukgolven in gelatine bij inslag van een projectiel", trainee report, Delft University of Technology, in Dutch.
- [23] Bree, J. (1999): "Impact duration of soft rubber bullet", personal communication.
- [24] Bolduc, M. and S. Tytko (1998): "Hybrid III head response to undefeated combat helmet in a ballistic environment", presented at the 2nd meeting of the NATO Task Group: Behind Armour Blunt Trauma, Colchester, UK.